

Growth cone navigation in substrate-bound ephrin gradients

Anne C. von Philipsborn^{1,2}, Susanne Lang¹, Jürgen Loeschinger¹, André Bernard³, Christian David⁴, Dirk Lehnert², Friedrich Bonhoeffer^{1,*} and Martin Bastmeyer^{2,*}

Graded distributions of ephrin ligands are involved in the formation of topographic maps. However, it is still poorly understood how growth cones read gradients of membrane-bound guidance molecules. We used microcontact printing to produce discontinuous gradients of substrate-bound ephrinA5. These consist of submicron-sized protein-covered spots, which vary with respect to their sizes and spacings. Growth cones of chick temporal retinal axons are able to integrate these discontinuous ephrin distributions and stop at a distinct zone in the gradient while still undergoing filopodial activity. The position of this stop zone depends on both the steepness of the gradient and on the amount of substrate-bound ephrin per unit surface area. Quantitative analysis of axon outgrowth shows that the stop reaction is controlled by a combination of the local ephrin concentration and the total amount of encountered ephrin, but cannot be attributed to one of these parameters alone.

KEY WORDS: Axon guidance, Microcontact printing, Retinotectal projection, Chick

INTRODUCTION

Axonal pathfinding plays an important role in the development of the complex connectivity of the nervous system. The correct navigation of axons to their target region is based on specific interactions with guidance factors, many of which are distributed in a graded way (Dickson, 2002). Indeed, gradients can provide positional information over a comparatively large area and are therefore suitable for the establishment of topographic maps (McLaughlin and O'Leary, 2005).

One of the best-studied examples of gradient-dependent axonal guidance is the retinotectal projection. In the chick, retinal ganglion cells (RGCs) from the temporal half of the retina project to the anterior part of the optic tectum, whereas nasal RGCs project to the posterior part. This topographic order has been shown to be mediated by a nasal to temporal expression gradient of EphA receptors in the retina and a complementary anterior to posterior expression gradient of repellent ephrinA ligands in the tectum (Drescher et al., 1995; Cheng et al., 1995; Connor et al., 1998).

Although extensive in-vitro and in-vivo data exist about this mode of topographic mapping (Brown et al., 2000; Feldheim et al., 2000; Feldheim et al., 2004), it is still poorly understood how retinal growth cones read gradients of repellent guidance molecules such as ephrinAs and integrate the information into a meaningful response. Several theoretical models have addressed the question of how growth cones read gradients and recognize their specific target areas in order to form a topographic map (Gierer, 1983; Honda, 1998; Goodhill and Urbach, 1999; Löschinger et al., 2000).

Experimentally, axonal guidance has been studied previously in diffusible gradients of soluble, secreted molecules, which induce growth cone turning (Lohof et al., 1992; Song et al., 1997), and in three-dimensional collagen gels (Rosoff et al., 2004). There is

evidence that growth cones can adjust their sensitivity to various concentrations of guidance factors in diffusible gradients (Ming et al., 2002; Piper et al., 2005). This continuous adaptation process, however, raises the question of how growth cones know when to stop in a gradient of repellent molecules. Moreover, in the in-vivo situation, RGC axons have to invade the repulsive ephrinA gradient in the tectum up to a certain point to find their target region rather than respond with negative turning angles as observed in the diffusible in-vitro gradients of repellents.

Few data exist about substrate-bound gradients, which represent an in-vivo-like experimental setup for ephrins, because their membrane attachment and/or clustering is required for proper Eph-receptor activation (Davis et al., 1994; Egea et al., 2005).

In the present study, we used microcontact printing (μ CP) of proteins to produce geometrically defined gradients of substrate-bound recombinant ephrinA5 in a reproducible and precise manner. By contrast to diffusible gradients, and in a similar way to gradients in collagen gels (Rosoff et al., 2004), microcontact-printed gradients are stable over a long time and can be designed in various shapes. This makes it possible to address directly the crucial question of how growth cones evaluate different parameters of a gradient, such as slope, local concentration and the total amount of encountered repellent molecules, and detect where to stop within the repellent gradient.

While Baier and Bonhoeffer first proposed that growth inhibition of temporal RGC axons is correlated with the maximal slope of a gradient (Baier and Bonhoeffer, 1992), subsequent experiments suggested, by contrast, that axons avoid a certain threshold concentration when they are faced with gradients of repellent membrane material (Rosentreter et al., 1998).

Our results indicate that growth cones integrate the slope and the local concentration in a gradient of repellent molecules. Based on these findings, we hypothesize that a combination of summation of encountered ephrin and adjustment to the local ephrin concentration enables the growth cone to read positional information and react to it in a meaningful way.

MATERIALS AND METHODS

Design of gradients and constant stripe patterns

Five linear gradients of different steepness were created as follows: the steepest gradient (relative steepness 1) consisted of an array of protein-covered stripes with constantly increasing width. The first stripe was 0.3 μ m wide and each

¹Max-Planck-Institut für Entwicklungsbiologie, Spemannstrasse 35, 72076 Tuebingen, Germany. ²Universität Karlsruhe (TH), Zoologisches Institut I, Zell- und Neurobiologie, Haid-und-Neu-Strasse 9, 76131 Karlsruhe, Germany. ³Institut für Mikro- und Nanotechnologie, Interstaatliche Hochschule für Technik Buchs NTB, Werdenbergstrasse 4, CH-9471 Buchs, Switzerland. ⁴Labor für Mikro- und Nanotechnologie, Paul Scherrer Institut, CH-5232 Villigen-PSI, Switzerland.

* Authors for correspondence (e-mail: friedrich.bonhoeffer@tuebingen.mpg.de; bastmeyer@bio.uka.de)

following stripe was $0.3\ \mu\text{m}$ wider than the one before. The lower edges of the stripes had the constant distance of $7.5\ \mu\text{m}$, i.e. the gaps between the stripes decreased in width. After 33 stripes, i.e. $247.5\ \mu\text{m}$, the stripe pattern merged into a homogeneously covered area. For stability reasons, there was a 1-mm-long array of dots with the edge length of $1\ \mu\text{m}$ in front of the gradient. The distance between the dots was $20\ \mu\text{m}$ along both the x - and y -axes.

Shallower gradients were created by disruption of the stripes. In gradients with the relative steepness $2/3$, the stripes were disrupted by $1\text{-}\mu\text{m}$ -long gaps every $3\ \mu\text{m}$, i.e. $1\text{-}\mu\text{m}$ -long gaps alternated with $2\text{-}\mu\text{m}$ -long protein-covered segments of the stripes.

Correspondingly, the gradients with the relative steepness $1/3$ consisted of gaps of $2\ \mu\text{m}$ between stretches of protein with a length of $1\ \mu\text{m}$, etc. (compare Fig. 1).

Three non-graded patterns with stripes of constant width ($0.3\ \mu\text{m}$, $0.6\ \mu\text{m}$ and $1.8\ \mu\text{m}$) were designed. As in the gradients, the lower edges of the stripes had the constant distance of $7.5\ \mu\text{m}$.

Stamping protein pattern fields

For μCP (Bernard et al., 2000; Quist et al., 2005), silicon masters with patterns described above were fabricated by low voltage electron beam lithography using a positive tone resist (David and Hambach, 1999). The resulting resist pattern was inverted using a lift-off process and reactive ion etching (David and Souvorov, 1999) to yield a master with rectangular, 650-nm -deep holes in the silicon surface.

Cuboids of polydimethylsiloxane (PDMS) were coated with ephrin solution, incubated for 20–30 minutes at 37°C , washed twice in ddH_2O and dried with a stream of N_2 . The protein-covered cuboid surface was then placed onto the silicon master and removed immediately. This way, the pattern of the master was transferred to the PDMS cuboid, which was then used as a stamp on glass coverslips. After the printing process, the coverslips were coated with $20\ \mu\text{g/ml}$ laminin (Invitrogen) in PBS for 30 minutes, washed in Hanks' medium and equilibrated with F12 medium.

As ink for μCP , a PBS solution containing $8\ \mu\text{g/ml}$ recombinant ephrinA5-Fc chimera protein (R&D Systems) clustered with $24\ \mu\text{g/ml}$ Alexa Fluor 488 anti-human Fc antibody (Molecular probes) was used. Alternatively, $16\ \mu\text{g/ml}$ ephrinA5-Fc was clustered with $48\ \mu\text{g/ml}$ antibody. To obtain less concentrated ephrin solutions (2 and $4\ \mu\text{g/ml}$), the clustered $8\ \mu\text{g/ml}$ standard solution was diluted with antibody clustered Fc. Clustered Fc at $8\ \mu\text{g/ml}$ was also used for control experiments.

For single experiments, recombinant ephrinA2-Fc chimera protein (R&D Systems) was used instead of ephrinA5.

The ephrin concentration per surface area in μCP gradients can be varied by either variation of the geometry of the gradient pattern or variation in the concentration of the printing ink. In the range of $2\text{--}8\ \mu\text{g/ml}$, the fluorescence

intensity of stamped ephrin increases roughly linear with the printing ink concentration. However, we cannot determine if the concentration of the printing ink is directly proportional to the amount of functional ephrin transferred to the coverslip. We therefore evaluate data from different printing ink concentrations separately.

Preparation, fixation and staining of retinal ganglion cell cultures

RGCs were dissected and cultured according to the method previously described (Walter et al., 1987). Briefly, retinae of embryonic day (E) 6–7 chick embryos were dissected in Hanks' medium and cut along the dorsoventral axis in $275\text{-}\mu\text{m}$ -wide stripes. The retinal stripes from either the temporal or the nasal half of the retina were placed approximately $700\text{-}\mu\text{m}$ in front of the protein patterns on the coverslips and grown in F12 medium containing 0.4% methylcellulose, 2% chicken serum and 5% fetal calf serum (FCS).

After 24 hours, the RGC cultures were fixed for 30 minutes in 4% paraformaldehyde/ 0.1% glutaraldehyde in PBS containing $0.3\ \text{mol/l}$ sucrose and stained with Alexa Fluor 594 phalloidin (Molecular Probes). Cultures were embedded in mowiol and photographed with an inverted phase contrast microscope (Axiovert 10, Zeiss) and a color video camera (Sonic CCD) using Analysis D software (Soft Imaging Systems). The acquired pictures were further processed with Photoshop CS software (Adobe).

Time-lapse microscopy

For time-lapse microscopy, μCP was performed onto surface-treated polystyrene cell culture dishes (Nunc). Time-lapse films were recorded with the microscope using $20\times$ and $63\times$ objectives and the camera system described above.

Quantitative evaluation of axonal growth

The acquired pictures were further processed with Photoshop CS software, to combine phase contrast pictures and pictures of fluorescently stained protein or two pictures with different fluorescence stainings.

For quantitative evaluation of axonal growth, the fluorescence of the anti-Fc antibody labeling the substrate-bound ephrin and the fluorescence of the phalloidin-stained axons were measured in a $495\ \mu\text{m} \times 375\ \mu\text{m}$ field containing the stamped pattern and a $100\text{-}\mu\text{m}$ -long area preceding the pattern. For this, a $10\text{-}\mu\text{m}$ -high measuring rectangle extending over the whole width of the field ($495\ \mu\text{m}$) was moved in $0.65\text{-}\mu\text{m}$ steps in the direction of axonal growth, i.e. rectangular to the gradient over the field, resulting in 553 data points along the vertical axis for each ephrin and axonal fluorescence. The intensity of axonal fluorescence was plotted against the distance overgrown by the axons, resulting in curves that reflected the distribution of axons and growth cones in the printed pattern and in the

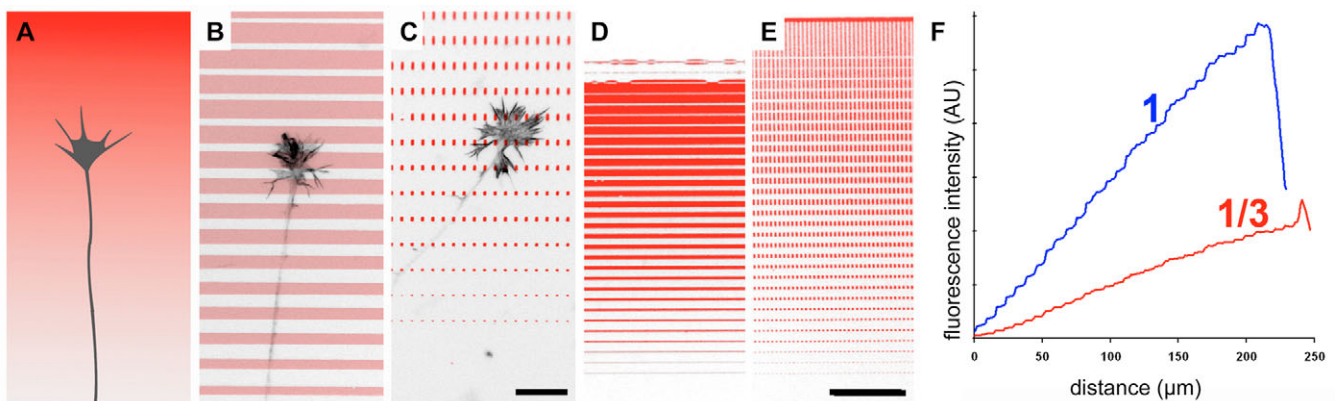


Fig. 1. Substrate-bound gradients fabricated by microcontact printing. (A) Schematic of a growth cone in a continuous gradient. (B,C) Growth cones in different discontinuous gradients fabricated by microcontact printing: (B) a steep gradient built by an array of stripes and (C) a shallow gradient built by dots. Antibody-stained ephrin is shown in red; phalloidin-stained actin in black. (D,E) The gradients shown in B and C in lower magnification extend over a distance of $250\ \mu\text{m}$. The relative slope 1 of the gradient in D is reduced to $1/3$ in E by interrupting the ephrin stripes. (F) Averaged fluorescence intensities measured in a $20\text{-}\mu\text{m}$ -wide measuring field moved along the axis of the gradients in D (blue curve) and E (red curve). Scale bars: $15\ \mu\text{m}$ in B,C; $50\ \mu\text{m}$ in D,E.

preceding area. After subtraction of the background fluorescence, curves were smoothed by calculation of the rolling average over 61 data points and were normalized for better comparison.

In normalized curves, each of the 493 overlapping $10\ \mu\text{m} \times 495\ \mu\text{m}$ measuring fields along the vertical axis of the gradient and the preceding area is assigned to the percentage of axonal fluorescence relating to the overall axonal fluorescence in the $495\ \mu\text{m} \times 375\ \mu\text{m}$ field. To obtain a mean growth curve for each gradient type, the growth curves of the single experiments were summed up and divided by the number of experiments. As a reference, curves were compared with the arithmetic mean of the relative fluorescence, which is calculated by dividing 100 by the number of 493 smoothed data points. The mean stop point position in each pattern was defined as the intersection between the mean growth curve and the arithmetic mean. The standard error of the mean stop point position was calculated based on the stop points of the single experiments. For the mean stop point positions in the $2\text{-}\mu\text{g/ml}$ gradient with the relative slope $1/6$, as well as in the three $2\text{-}\mu\text{g/ml}$ non-graded patterns, no standard error could be calculated because the growth curves of some single experiments displayed several intersection points with the arithmetic mean.

ANOVA was applied to the mean stop points in gradients with different slope and non-graded patterns with different stripe widths, respectively. Student's *t*-test was used to compare the mean stop points in gradients with the same slope but printed with two different ephrin concentrations (4 and 8 $\mu\text{g/ml}$).

RESULTS

Fabrication of substrate-bound ephrin gradients by microcontact printing

Patterns fabricated by μCP consist of dots and lines, which are printed with a fixed printing ink concentration, but vary with respect to their sizes and spacings. By contrast to continuous gradients with smooth transitions between different concentrations (Fig. 1A), these gradients are discontinuous (Fig. 1B-E). In the present study, we used solutions of human ephrinA5-Fc protein, which was preclustered with fluorescently labeled anti-human Fc antibody as printing ink, and coated the glass or plastic surface with laminin as a growth-promoting molecule.

The steepest gradient produced in this way consisted of an array of protein-covered stripes with constantly increasing width ($0.3\ \mu\text{m}$ per stripe) (Fig. 1D,E). The distance between the upper edges of the stripes was constant ($7.5\ \mu\text{m}$). Shallower gradients were created by interruptions of the stripes (Fig. 1C,E). Microcontact-printed ephrin gradients are highly reproducible, stable and biologically active. The ephrin coverage at different positions of the gradient could be easily

quantified by measuring the fluorescence intensity of the antibody used for clustering. In Fig. 1F, the average fluorescence intensities within a $20\text{-}\mu\text{m}$ measuring field were plotted against the longitudinal axis of the two gradients shown in Fig. 1D,E. In both gradients, the fluorescence intensity increased in a linear way with distance and was directly proportional to the ephrin coverage given by the geometry of the graded pattern. As the average diameter of a chick RGC growth cone is $15\text{-}20\ \mu\text{m}$, it can be assumed that a growth cone overgrowing these discontinuous gradients faces a more or less linear increase of ephrin coverage.

Temporal RGC growth cones form defined stop zones in ephrin gradients

RGC axons from the nasal retinal half grew over the ephrin gradient without being repelled or displaying a stop reaction. In cultures fixed after 24 hours, nasal growth cones were distributed evenly over the gradient and decreased only slightly in density with increasing distance from the retinal explant (Fig. 2A).

By contrast, growth cones from the temporal retina invaded the beginning of the gradient, but did not advance beyond a distinct range. They built up a stable stop zone consisting of a dense meshwork of axons, growth cones and thickened axons shafts (Fig. 2B). Around 5-10% of the temporal axons did not stop in the ephrin gradient. As in earlier studies (Rosentreter et al., 1998; Monschau et al., 1997), no graded response was visible along the naso-temporal axis of the temporal half of the retina.

In control experiments, where Fc protein was used instead of ephrin for fabrication of the gradient, both temporal and nasal axons crossed the gradient without stopping (data not shown).

The reaction of individual temporal growth cones within ephrin gradients was observed by time-lapse microscopy (Fig. 3; see Movie 1 in the supplementary material). Temporal growth cones invaded shallow gradients without major changes in morphology (Fig. 3A). Within the gradient, phases of transient retraction alternated with phases of elongation until the growth cone stopped at a defined position. While pausing in that relatively small area, the growth cone constantly rearranged its filopodia and lamellipodia, actively exploring its environment. In the steepest ephrin gradient, reactions of temporal growth cones were more pronounced (Fig. 3B). Nasal growth cones grew over ephrin patterns without pausing or retracting. The same was true for temporal growth cones growing within Fc gradients (data not shown).

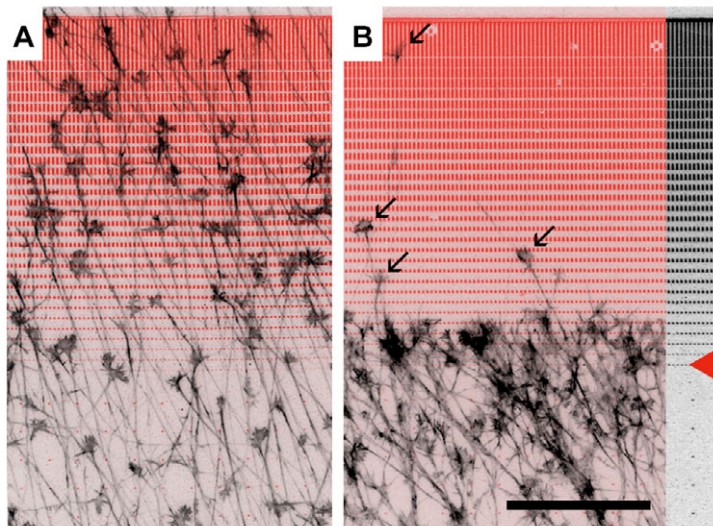


Fig. 2. Temporal, but not nasal, RGC axons form stop zones in ephrin gradients. (A) Nasal growth cones overgrow an ephrin gradient without being affected. (B) By contrast, temporal growth cones form a distinct stop zone in the ephrin gradient. As new axons continuously leave the explant, growth cones are observed in the area between the explant and the stop zone. Arrows mark growth cones that do not respond to the gradient. To the right, the ephrin gradient is shown in black with a red arrowhead marking the beginning of the gradient. Antibody-stained ephrin is shown in red; phalloidin-stained actin in black. Scale bar: $100\ \mu\text{m}$.

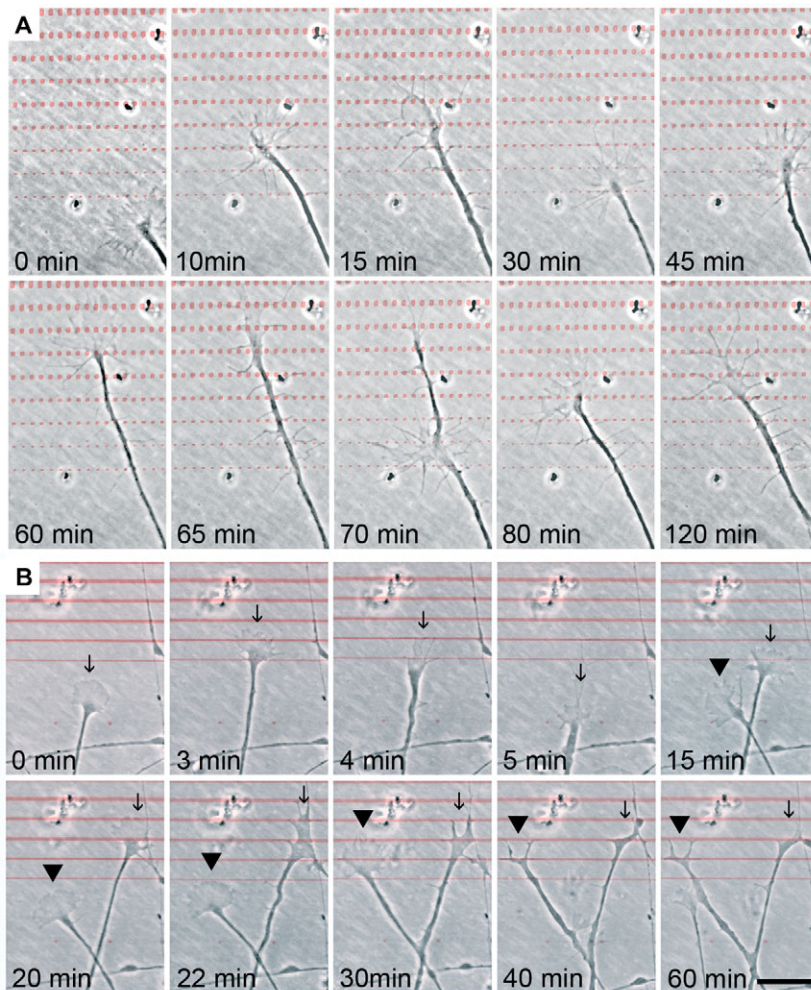


Fig. 3. Growth cone dynamics within the stop zone of shallow and steep gradients. (A) Growth cones display an explorative equilibrium of forward and backward movements within the stop zone of a shallow gradient. A temporal growth cone approaches the gradient. After 15 minutes it pauses, rearranges its lamellipodia and starts to retract to the beginning of the gradient (30 minutes). Between 45 and 60 minutes the growth cone advances anew in the gradient and subsequently pauses (65 minutes). Small side branches appear along the axon shaft and a growth cone like structure builds at the beginning of the gradient (70 minutes). The axon shaft left deeper in the gradient retracts. Between 80 and 120 minutes the growth cone pauses under continued filopodial activity within the gradient. (B) Steep ephrin gradients can cause more pronounced reactions, including transient, partial growth cone collapse and change of growth cone morphology within the stop zone. A temporal growth cone entering a steep gradient starts withdrawing its lamellipodia (4 minutes), and retracts completely from the gradient (5 minutes). After 15 minutes the growth cone marked by an arrow recovers from the transient collapse and invades the gradient anew. A second growth cone (arrowhead) advances. Between 20 and 22 minutes the growth cone marked by an arrow undergoes a rapid change in morphology and realigns its filopodia along the printed ephrin pattern. The same happens to the growth cone marked by an arrowhead between 20 and 30 minutes. Afterwards, both growth cones remain stationary and undergo only small morphological changes, adhering partially to the lines of the gradient. Antibody-stained ephrin is shown in red; axons are shown in phase contrast. Scale bar: 20 μm .

These findings suggest: (1) that temporal growth cones can detect patterns as gradients, although they are discontinuous at the microscale, and are able to integrate patchy ephrin distributions in the range of several micrometers; and (2) that substrate-bound ephrin provokes not only repulsion and retraction, but can also elicit growth cone stop at a defined position within the gradient.

Stable axonal stop zones can be broken down by addition of soluble ephrin

Our time-lapse studies indicate that the stop reaction of temporal axons within the ephrin gradient is not a permanent growth cone collapse or adhesion to high amounts of substrate-bound ephrin, but rather a dynamic process. To interfere with Eph-receptor/ephrin-ligand interactions, soluble dimeric ephrin was added to the culture medium. Soluble dimeric ephrin has been shown previously to have a repulsive effect on retinal growth cones (Weinl et al., 2003). After adding 500 ng/ml soluble ephrinA5-Fc protein to temporal RGCs growing on laminin, we observed transient growth cone collapse followed by retraction during the first 0.5-1 hours. After this time, growth cones resumed forward elongation at the same rate as before addition of ephrin (data not shown). When temporal axons were grown from the beginning in medium containing 250-500 ng/ml soluble ephrin, stop zones never formed and cultures were indistinguishable from Fc controls (data not shown). We next added soluble ephrinA5 at a concentration of 500 ng/ml to cultures of temporal axons a few hours after a visible stop zone had formed.

After 1 hour, a subset of axons overshot the stop zone, which disappeared almost completely after 2 hours. During disappearance of the stop zone, axons with stationary growth cones resumed elongation and stop reactions of newly advancing growth cones were abolished. Addition of 500 ng/ml soluble Fc did not affect the stop reaction (data not shown).

These findings demonstrate that the growth cones pausing within the stop zone remain active and that the stop reaction is reversible.

Temporal RGC axons elongate differently in ephrin gradients of different slope

Given that temporal growth cones stop reproducibly at a defined zone in ephrin gradients, we further addressed the question of how the position of this stop zone would vary in gradients of different slope and in gradients containing different amounts of ephrinA5. The geometrical design of the printing stamps allowed us to fabricate five linear gradients with relative slopes of 1, 2/3, 1/2, 1/3 and 1/6. The absolute concentration of ephrinA5 in the gradients was varied by using different ephrin concentrations (2, 4, 8 and 16 $\mu\text{g/ml}$) in the printing ink. In some experiments, ephrinA5 was replaced by ephrinA2. As we did not observe any obvious differences in the axonal reaction (data not shown), only ephrinA5 was further used throughout the study.

Fig. 4A shows three gradients with the relative slopes of 1, 2/3 and 1/3 printed with 8 $\mu\text{g/ml}$ ephrinA5. With decreasing slope, the stop zone proceeded deeper into the gradient. For a precise quantification

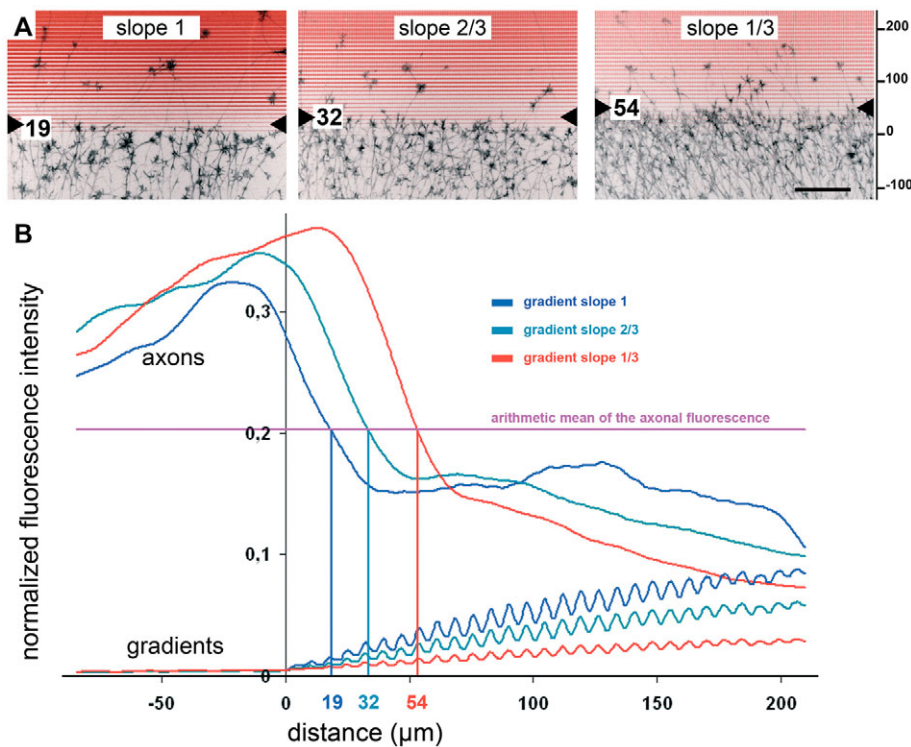


Fig. 4. The position of the stop zone depends on the slope of the gradient. (A) Temporal axons in three different gradients printed with 8 $\mu\text{g/ml}$ ephrinA5. Antibody-stained ephrin is shown in red; axonal actin in black. In the steepest gradient (relative slope 1) the stop zone is located at the beginning of the gradient. In shallower gradients (relative slopes 2/3 and 1/3), stop zones are shifted deeper into the gradient. The position of the stop zone is marked with arrowheads and the overgrown distance within the gradient is indicated in μm . The axis to the right (in μm) corresponds to the x-axis in B. Scale bar: 100 μm . (B) Standardized fluorescence intensity curves of ephrin and the corresponding axonal fluorescence are depicted in blue (gradient slope 1), light blue (2/3) and red (1/3). The discontinuity of the gradient reflects in the sinuous course of the ephrin fluorescence intensity curve. The x-coordinate of the intersection of each axonal curve with the arithmetic mean (pink line) is defined as the position of the stop zone. The shallower the gradient, the further the stop zone is shifted in the direction of the positive x-axis.

of the distribution of growth cones and the position of the stop zone in the gradient, the actin in growth cones and axons was stained with fluorescently labelled phalloidin. The fluorescence intensity was measured in a standardized field encompassing the gradient and was plotted against the distance traveled by the axons. The resulting curves reflect the density of axons and growth cones at each point along the gradient (Fig. 4B). The position of the axonal stop zone was defined as the point along the axis of the gradient where the axonal fluorescence drops below the arithmetic mean of the overall axonal fluorescence for the first time (for details see Materials and methods). As shown in Fig. 4, the position of the stop zone determined in this way corresponded well with the stop zone position estimated by visual inspection. As the even distribution of temporal axons growing on Fc protein gradients led to curves that were roughly equal to the arithmetic mean line (Fig. 5A), we chose the arithmetic mean as a reference.

Axonal growth curves from several experiments were averaged for each gradient type. Steeper gradients, as well as a higher printing ink concentration, led to lower stop zone positions (Fig. 5A,B). As shown in Fig. 5C, the relative slope of the gradient and the position of the stop zone correlated linearly for all three printing ink concentrations. In gradients printed with 2 $\mu\text{g/ml}$ ephrin solution, axons formed a diffuse stop zone, located deep in the gradient, suggesting that 2 $\mu\text{g/ml}$ is near the lower limit of the printing ink concentration sufficient to elicit a stop reaction. Although the standard error of the mean stop zone position is high, the data points for 2- $\mu\text{g/ml}$ gradients show the same trend as the statistically firm data from 4- and 8- $\mu\text{g/ml}$ gradients (Fig. 5C).

An increase of the printing ink concentration to 16 $\mu\text{g/ml}$ did not significantly change the stop zone positions observed for 8 $\mu\text{g/ml}$ (data not shown), suggesting that either maximal reactivity of the axons or maximal surface coverage is reached in 8- $\mu\text{g/ml}$ gradients.

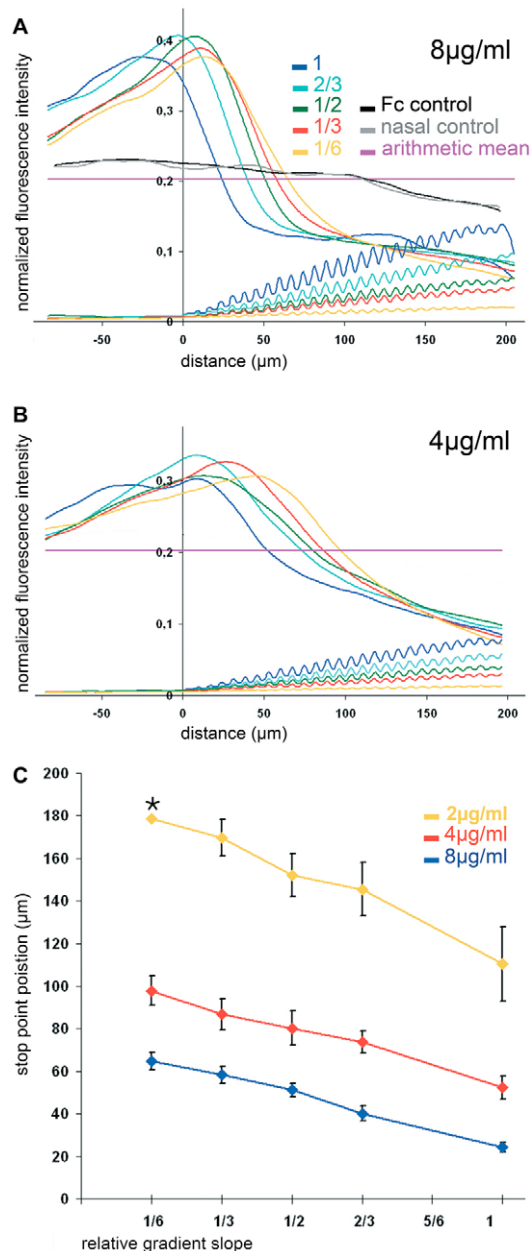
The magnitude of axonal outgrowth did not affect the stop point position in our experimental setup (data not shown).

These results show that temporal growth cones can distinguish different slopes and discriminate between different protein concentrations of ephrinA5 at given slopes.

Temporal axons stop in non-graded ephrin patterns

Starting from the observation that stop zone positions depend on the slope of the gradient and the ephrin concentration, we asked what determines the position of the stop zone in an individual gradient and what are common parameters of all stop zone positions in the different gradients. In the simplest case, one would envisage that growth cones stop at a fixed local concentration, which is reached earlier in steeper gradients and later in shallower gradients. To test this hypothesis, three discontinuous non-graded patterns were built by an array of stripes with the constant thickness of 0.3, 0.6 and 1.8 μm . If only the local ephrin concentration determines the stop reaction, temporal axons would either not enter these patterns or continue their growth without being affected. Surprisingly, temporal axons reacted to non-graded ephrin patterns as to linear gradients. After overgrowing a certain distance in the pattern, growth cones stopped and formed a distinct stop zone (Fig. 6A). The thicker the stripes of the pattern, or the higher the printing ink concentration, the earlier the axons formed a stop zone (Fig. 6B).

The observed axonal stop reaction in non-graded ephrin patterns indicates that the local ephrin concentration does not solely determine the stop point position and suggests an additional summation mechanism within a growth cone. We therefore estimated the total amount of ephrin a growth cone has encountered on its way to the stop zone by summing the area of the ephrin covered spots in a 15 μm wide rectangle spanning from the beginning of the pattern up to the stop zone (Fig. 7A, left). In addition, the local ephrin concentration at the stop zone position was determined as the percentage of ephrin coverage in a measuring square of 15 \times 15 μm (Fig. 7A, right). Both the local ephrin concentration and the total amount of ephrin encountered on the way



to the stop zone varied, depending on the pattern. When these two parameters were plotted against each other for all graded and non-graded patterns (Fig. 7B), a linear correlation became apparent. Equations for the linear smoothing functions are: $y=2.8x + 13.0$ with the correlation coefficient $R=0.89$ (8 μg/ml), $y=4.4x + 33.5$, $R=0.81$ (4 μg/ml) (Fig. 7B) and $y=9.7x + 58.8$, $R=0.97$ (2 μg/ml) (data not shown). In shallow gradients, as well as in non-graded patterns with thin stripes, both the local ephrin concentration and the total encountered ephrin-covered area were lower than in steep gradients and non-graded patterns with thick stripes. From this we conclude that the pattern in which ephrin is presented to the growth cone influences the efficiency of the transmitted stop signal.

DISCUSSION

Using μCP, we generated stable and precise gradients of substrate-bound ephrin protein. We found that temporal RGC axons reacted to these gradients by forming stop zones, but remained responsive

Fig. 5. Quantification of average axonal stop zones in different gradients. (A,B) The two graphs show the averaged axonal growth curves for five gradients printed with 8 μg/ml (A) or 4 μg/ml (B). The relative slope of the gradients is indicated with the colour code given in A. In A, the averaged curve of Fc controls is shown in black, the curve of nasal controls in gray and the arithmetic mean of the axonal fluorescence in pink. For both ephrin concentrations axonal curves intersect the arithmetic average later the shallower the gradient is. Curves in B intersect the arithmetic mean later than curves in A. The axonal curves were averaged from $n=7$ (gradient slope 1/6), $n=8$ (1/3), $n=9$ (1/2), $n=5$ (2/3), $n=6$ (1), $n=10$ (Fc controls), $n=5$ (nasal controls) experiments in A, and from $n=9$ (1/6), $n=9$ (1/3), $n=8$ (1/2), $n=13$ (2/3), $n=7$ (1) experiments in B. Mean stop point positions are 64.9 ± 4.2 μm (1/6), 58.3 ± 3.9 μm (1/3), 51.2 ± 3.1 μm (1/2), 40.2 ± 3.6 μm (2/3), 24.4 ± 2.2 μm (1) in A and 97.9 ± 6.8 μm (1/6), 86.8 ± 7.3 μm (1/3), 80.3 ± 8.0 μm (1/2), 73.8 ± 5.1 μm (2/3), 52.3 ± 5.5 μm (1) in B. (C) Plotting the stop point positions determined in A and B and stop point positions in gradients printed with 2 μg/ml against the relative slope of the corresponding gradients shows that the two parameters correlate in a linear way. Error bars indicate the standard error. Mean stop positions in gradients printed with 2 μg/ml are: 178.8 μm (1/6, $n=4$), 169.6 ± 8.5 μm (1/3, $n=5$), 152.0 ± 10.2 μm (1/2, $n=5$), 145.5 ± 12.4 μm (2/3, $n=5$), 110.3 ± 17.5 μm (1, $n=5$). Due to the data examination method, no standard error could be calculated for the mean stop point position in the gradient with the slope 1/6 (marked with a star, for details see Materials and methods). $P < 0.002$ by ANOVA for both of the two groups of 8 μg/ml and 4 μg/ml gradients and $P < 0.156$ for 2 μg/ml gradients. Student's *t*-test was applied to compare the mean stop points in gradients with the same slope but printed with 8 μg/ml and 4 μg/ml: $P < 0.002$ (gradient slope 1/6), $P < 0.006$ (1/3), $P < 0.003$ (1/2), $P < 0.001$ (2/3), $P < 0.002$ (1).

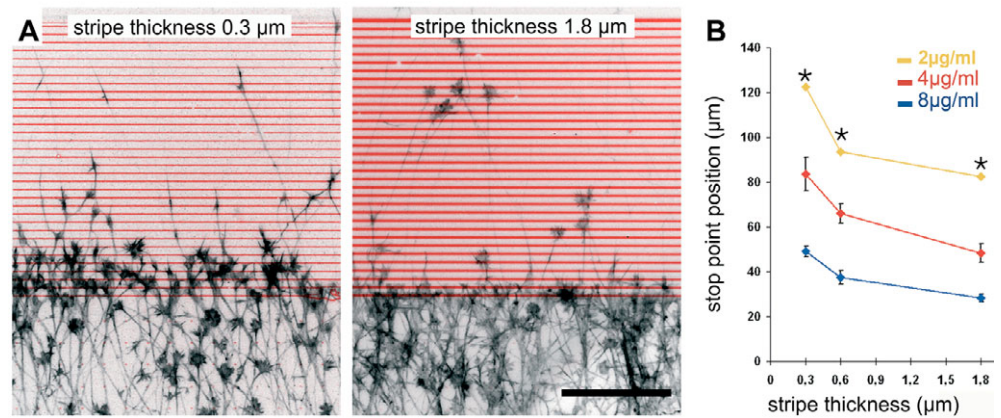
to signaling modulations. The stop reaction depended on the slope of the gradient and the absolute ephrin concentration, providing evidence for an integrative mechanism that enables growth cones to discriminate between different ephrin distributions.

By contrast to continuous gradients with smooth transitions between different concentrations, discontinuous gradients of substrate-bound ephrinA5 consist of submicron-sized protein-covered spots that vary with respect to their sizes and spacing but do contain the same amount of ephrin per surface unit. Although quantitative measurements of in-situ signals for ephrinAs give the impression of a continuous gradient within the tectum (Drescher et al., 1995; Cheng et al., 1995), retinal axons might in vivo be confronted with gradients of guidance molecules discontinuous on a microscale. Studies in the regenerating visual system of goldfish suggest that the tectal ephrinA2 gradient is built by increasing numbers of ephrinA2-expressing tectal cells with similar ephrin expression levels (King et al., 2004). In the chick tectum, growth cones are confronted with intermingled processes of neurons, glial cells and radial glial endfeet, which express ephrinAs at different levels (Davenport et al., 1998).

Proper EphA/ephrinA signaling is dependent on cleavage and internalization of ephrinA (Hattori et al., 2000; Janes et al., 2005). As this cleavage has been shown recently to occur in trans (Janes et al., 2005), it can be assumed to take place in our system, where ephrinA5 is bound to the surface.

Topographic mapping is thought to be based on a graded responsiveness of retinal growth cones towards ephrin along the naso-temporal axis of the retina (McLaughlin and O'Leary, 2005). However, we found, in accordance with previous in-vitro studies

Fig. 6. Temporal axons stop in non-graded striped ephrin patterns. (A) Stop zones of temporal axons in non-graded patterns printed with 8 $\mu\text{g/ml}$ ephrinA5. Antibody-stained ephrin is shown in red; phalloidin-stained axonal actin in black. In the pattern consisting of 0.3 μm thick stripes, growth cones stop later than in the pattern of 1.8 μm stripes. Scale bar: 100 μm . (B) The position of the axonal stop points in three different stripe patterns is plotted against the stripe thickness for patterns printed with 8, 4 and 2 $\mu\text{g/ml}$.



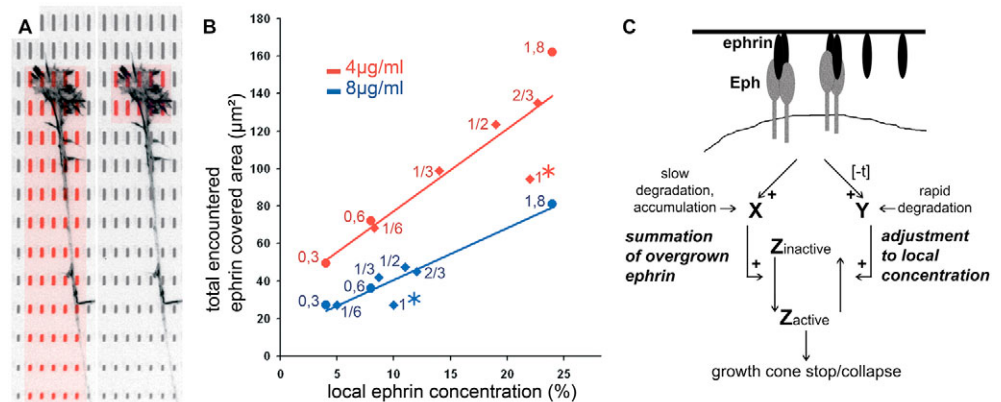
Mean stop points were $49.1 \pm 2.3 \mu\text{m}$ (stripe thickness 0.3 μm , $n=5$), $37.4 \pm 3.0 \mu\text{m}$ (0.6 μm , $n=6$), $28.3 \pm 1.7 \mu\text{m}$ (1.8 μm , $n=6$) for 8- $\mu\text{g/ml}$ patterns, $83.7 \pm 7.8 \mu\text{m}$ (0.3 μm , $n=6$), $66.0 \pm 4.3 \mu\text{m}$ (0.6 μm , $n=7$), $48.8 \pm 4.2 \mu\text{m}$ (1.8 μm , $n=10$) for 4 $\mu\text{g/ml}$ patterns and 122.4 μm (0.3 μm , $n=2$), 93.7 μm (0.6 μm , $n=3$), 82.6 μm (1.8 μm , $n=3$) for 2 $\mu\text{g/ml}$ patterns. Error bars indicate standard error. Due to the data examination method, no standard error could be calculated for the mean stop point position in the patterns printed with 2 $\mu\text{g/ml}$ (marked with stars, for details see Materials and methods). $P < 0.001$ by ANOVA for 8 $\mu\text{g/ml}$ patterns and $P < 0.006$ for 4 $\mu\text{g/ml}$ patterns. Student's t -test for small sample sizes was applied to compare the mean stop points in patterns with the same stripe thickness printed with 8 and 4 $\mu\text{g/ml}$: $P < 0.001$ (stripe thickness 0.3 μm), $P < 0.001$ (stripe thickness 0.6 μm), $P < 0.003$ (stripe thickness 1.8 μm).

(Baier and Bonhoeffer, 1992; Walter et al., 1987), that all temporal growth cones reacted as a uniformly responsive population and all nasal growth cones were unresponsive. In our experimental system, fiber-fiber interaction/competition among growth cones might be reduced compared to the in-vivo situation. As competition of retinal axons has been implicated in topographic mapping (Prestige and Willshaw, 1975; Brown et al., 2000; Feldheim et al., 2000; Feldheim et al., 2004; Honda, 2003; Honda, 2004), we cannot rule out that the omission of axon competition gives rise to the uniform behavior of all temporal axons in our experimental setup. The observed uniform behavior is more compatible with models in which gradients of ephrinAs in the target field act to sort out temporal and nasal axons, whereas retinotectal mapping is later produced by topographically specific interstitial branching (McLaughlin and O'Leary, 2005).

In a recent study, it was demonstrated that retinal axons show a graded response to ephrinAs (Hansen et al., 2004). EphrinA2 inhibited growth at high concentrations but promoted growth at low concentrations. The transition from promotion to inhibition varied along the naso-temporal axis of the retina. The experimental designs in this study differed at various points from the ones used here. Most notably, Hansen and co-workers cultured retinal explants directly on a uniformly covered ephrin substrate, whereas in our work RGC axons were confronted with a graded distribution of ephrinA5 after elongation on an ephrin-free stretch of way.

We found that both gradient slope and absolute ephrin concentration affected the position of the stop zone in a significant and reproducible way. In an earlier study, temporal axons were confronted with linear gradients of repellent membrane fragments

Fig. 7. A balance of summation of the total encountered ephrin and adjustment of sensitivity to the local ephrin concentration may lead to growth cone stop. (A) Schematic of the total amount of encountered ephrin in the gradient (red dots in the rectangle on the left) and local encountered ephrin (red dots in the rectangle on the right). (B) When the local ephrin concentration is plotted against the total encountered ephrin-covered area at the stop point for all patterns, a linear correlation becomes apparent. Blue data points are derived from patterns printed with 8 $\mu\text{g/ml}$, red data points from patterns printed with 4 $\mu\text{g/ml}$ ephrin printing ink. The relative slope of the gradient (1, 2/3, 1/2, 1/3, 1/6) or the thickness of the stripes in the non-graded patterns (1.8, 0.6, 0.3 μm) is noted next to the data point. Data points for gradients with the relative slope 1 (marked with stars) deviate noticeable from the linear smoothing function. For explanation, see text. (C) The correlation shown in B can be explained by a model in which the repulsive ephrin signal is summed up over time by accumulation of a slowly degrading signaling molecule X, which positively affects growth cone stop, retraction and/or collapse. Temporally delayed (Δt), a second, rapidly degrading component Y leads to an adjustment of the sensitivity to the local ephrin concentration, counteracting the output of X. The activity of X is postulated to be proportional to the total encountered ephrin, whereas the activity of Y is proportional to the local ephrin concentration. The growth cone stops when both activities are proportionable.



can be explained by a model in which the repulsive ephrin signal is summed up over time by accumulation of a slowly degrading signaling molecule X, which positively affects growth cone stop, retraction and/or collapse. Temporally delayed (Δt), a second, rapidly degrading component Y leads to an adjustment of the sensitivity to the local ephrin concentration, counteracting the output of X. The activity of X is postulated to be proportional to the total encountered ephrin, whereas the activity of Y is proportional to the local ephrin concentration. The growth cone stops when both activities are proportionable.

from either caudal tectum or ephrinA-expressing cell lines (Rosentreter et al., 1998). Here growth cones reacted to an apparent threshold concentration of repellent material that was independent of slope (Rosentreter et al., 1998). However, by contrast to the present study, axons did not stop once they reached the threshold concentration, but rather continued elongation on areas covered with low amounts of membrane material. The influence of the slope may be seen only after the precise quantification of the guidance molecules, which is possible in gradients fabricated by μ CP.

Although addition of soluble, dimeric ephrin leads to transient growth cone collapse and retraction, it is not sufficient for the more enduring stop observed in the patterns of substrate-bound ephrin. When added to an already formed stop zone, soluble ephrin caused the breakup of the stop zone and inhibited further stopping in the gradient. These observations might be explained in two ways. Firstly, in the signaling complexes of stopped growth cones, Eph receptors are continuously replaced by new receptors to ensure proper signaling. Soluble ephrin would then compete with substrate-bound ephrin for the EphA receptors on the growth cone. Secondly, soluble dimeric ephrin might induce a different axonal response from that of substrate-bound clustered ephrin. In both cases, signaling cascades of Eph receptors induced by higher order clusters (substrate-bound ephrin) and by soluble dimeric ephrin should differ, a phenomenon that has recently been demonstrated for the EphA4 receptor (Egea et al., 2005).

The local concentration at the stop zone varies in the different ephrin patterns, and therefore it cannot be claimed that it is the sole cause of the stop reaction. The same is true for the total amount of ephrin that a growth cone had encountered when it stopped at the stop zone. Interestingly, we find the local ephrin concentration and the total encountered ephrin-covered area at the stop point position correlated in a linear way for all tested ephrin patterns and printing ink concentrations (Fig. 7B). Based on these findings, we suggest a model where the local ephrin concentration and the total encountered ephrin-covered area have opposite effects on growth cone advance (Fig. 7C). We hypothesize that the stop tendency of the growth cone increases with the total encountered ephrin-covered area, whereas the local ephrin concentration is proportional to an adjustment process preventing the stop reaction. As soon as these parameters reach a certain ratio, the growth cone stops. On the intracellular level, summation of the overgrown ephrin and adjustment to the local ephrin concentration should be regulated via two different signal transduction pathways, which have opposite effects on a molecular switch (Z) regulating growth cone stop (Fig. 7C). Summation occurs via a component X, which is inactivated slowly and therefore accumulates. Adjustment, by contrast, is based on a component Y, which is rapidly inactivated, and so has levels that reflect the local ephrin concentration. The rise in levels of Y should be temporally delayed upon activation of EphA receptors, compared with levels of X.

A model that includes summation and adjustment mechanisms explains why axons stop at lower local concentrations in shallow gradients than in steep gradients and why stop zones form at all in non-graded discontinuous patterns. A temporal delay in the adjustment pathway could account for cycles of growth cone retraction/pausing alternating with elongation observed with time-lapse microscopy (Fig. 3A). This temporal delay can also explain why the ratio between the local ephrin concentration and the total encountered ephrin-covered area deviates noticeably from the linear smoothing function for gradients with the relative slope 1 printed with 4 and 8 μ g/ml (Fig. 7B, marked with stars), because in the steepest gradients the adaptation level may lag behind the actual local concentration.

Explorative forward movements alternating with retraction/pausing may be equivalent to the observed cycles of desensitization/resensitization, which have been conceptualized as a mode of adaptation (Ming et al., 2002; Piper et al., 2005). It should be noted, however, that recent work from the lab of G. Goodhill has questioned the requirement of adaptation for the response of axons to molecular gradients (Xu et al., 2005).

In a system in which the local ephrin concentration and the total encountered ephrin-covered area are integrated, the slope of the gradient has less impact on the overgrown distance than in a scenario in which growth cones would stop either at a fixed local concentration or after a fixed overgrown sum. In the in-vivo situation, such integrative mechanisms would be advantageous, as a moderate change in the gradient slope would not affect substantially the stop zone position, making the system robust and less susceptible to variances in ephrin expression levels.

In summary, we found that retinal growth cones can detect and integrate discontinuous gradients of substrate-bound ephrinA5 by forming a distinct stop zone within the gradient. The axonal reaction is controlled by a combination of the local ephrin concentration and the total encountered ephrin. Whether similar mechanisms are involved in the formation of the retinotopic map in vivo remains to be elucidated. Here growth cones are confronted with a much more complex environment, not only consisting of a single ephrinA5 gradient but also superimposed graded distributions of other ephrins and counter gradients of Eph-receptors (Connor et al., 1998; Feldheim et al., 2004). Gradients produced by microcontact printing, on all accounts, proved to be a useful tool to explore possible modes of gradient detection and integration by growth cones and other migrating cell types.

We thank A. Gierer, M. Pankratz and F. Weth for helpful comments on the manuscript. The authors are very grateful for friendly and helpful support by A. Lupas and his department at the Max Planck Institute for Development Biology in Tuebingen. This work was supported by the DFG (grant 1034/14-1 to M.B. and F.B.). A.P. receives a stipend from the German National Academic Foundation.

Supplementary material

Supplementary material for this article is available at <http://dev.biologists.org/cgi/content/full/133/13/2487/DC1>

References

- Baier, H. and Bonhoeffer, F. (1992). Axon guidance by gradients of a target-derived component. *Science* **255**, 472-475.
- Bernard, A., Renault, J. P., Michel, B., Bosshard, H. R. and Delamarque, E. (2000). Microcontact printing of proteins. *Adv. Mat.* **12**, 1067-1070.
- Brown, A., Yates, P. A., Burrola, P., Ortuno, D., Vaidya, A., Jessell, T. M., O'Leary, D. D. M. and Lemke, G. (2000). Topographically mapping from the retina to the midbrain is controlled by relative but not absolute levels of EphA receptor signaling. *Cell* **102**, 77-88.
- Cheng, H. J., Nakamoto, M., Bergemann, A. D. and Flanagan, J. G. (1995). Complementary gradients in expression and binding of ELF-1 and Mek4 in development of the topographic retinal projection map. *Cell* **82**, 371-381.
- Connor, R. J., Menzel, P. and Pasquale, E. B. (1998). Expression and tyrosine phosphorylation of Eph receptors suggests multiple mechanisms in patterning the visual system. *Dev. Biol.* **193**, 21-35.
- Davenport, R. W., Thies, E., Zhou, R. and Nelson, P. G. (1998). Cellular localization of ephrin-A2, ephrin-A5, and other functional guidance cues underlies retinotopic development across species. *J. Neurosci.* **18**, 975-986.
- David, C. and Hambach, D. (1999). Line width control using a defocused low voltage electron beam. *Microelec. Eng.* **46**, 219-222.
- David, C. and Souvorov, A. (1999). High-efficiency Bragg-Fresnel lenses with 100 nm outermost zone width. *Rev. Sci. Instrum.* **70**, 4168-4173.
- Davis, S., Gale, N. W., Aldrich, T. H., Maisonpierre, P. C., Lhotak, V., Pawson, T., Goldfarb, M. and Yancopoulos, G. D. (1994). Ligands for EPH-related receptor tyrosine kinases that require membrane attachment or clustering for activity. *Science* **266**, 816-819.
- Dickson, B. J. (2002). Molecular mechanisms of axon guidance. *Science* **298**, 1959-1964.
- Drescher, U., Kremoser, C., Handwerker, C., Lösinger, J., Noda, M. and

- Bonhoeffer, F.** (1995). In vitro guidance of retinal ganglion cell axons by RAGS, a 25kDa tectal protein related to ligands for Eph receptor tyrosine kinases. *Cell* **82**, 359-370.
- Egea, J., Nissen, U. V., Dufour, A., Sahin, M., Greer, P., Kullander, K., Mrcic-Flogel, T. D., Greenberg, M. E., Kiehn, O., Vanderhaeghen, P. et al.** (2005). Regulation of EphA4 kinase activity is required for a subset of axon guidance decisions suggesting a key role for receptor clustering in Eph function. *Neuron* **47**, 515-528.
- Feldheim, D. A., Kim, Y. I., Bergemann, A. D., Frisen, J., Barbacid, M. and Flanagan, J. G.** (2000). Genetic analysis of ephrin-A2 and ephrin-A5 shows their requirement in multiple aspects of retinocollicular mapping. *Neuron* **25**, 563-574.
- Feldheim, D. A., Nakamoto, M., Osterfield, M., Gale, N. W., DeChiara, T. M., Rohatgi, R., Yancopoulos, G. D. and Flanagan, J. G.** (2004). Loss-of-function analysis of EphA receptors in retinotectal mapping. *J. Neurosci.* **24**, 2542-2550.
- Gierer, A.** (1983). Model for the retino-tectal projection. *Proc. R. Soc. Lond. B Biol. Sci.* **218**, 77-93.
- Goodhill, G. J. and Urbach, J. S.** (1999). Theoretical analysis of gradient detection by growth cones. *J. Neurobiol.* **41**, 230-241.
- Hansen, M. J., Dallal, G. E. and Flanagan, J. G.** (2004). Retinal axon response to ephrin-As shows a graded, concentration-dependent transition from growth promotion to inhibition. *Neuron* **42**, 717-730.
- Hattori, M., Osterfield, M. and Flanagan, J. G.** (2000). Regulated cleavage of a contact-mediated axon repellent. *Science* **289**, 1360-1365.
- Honda, H.** (1998). Topographic mapping in the retinotectal projection by means of complementary ligand and receptor gradients: a computer simulation study. *J. Theor. Biol.* **192**, 235-246.
- Honda, H.** (2003). Competition between retinal ganglion axons for targets under the servomechanism model explains abnormal retinocollicular projection of Eph receptor-overexpressing or ephrin-lacking mice. *J. Neurosci.* **23**, 10368-10377.
- Honda, H.** (2004). Competitive interactions between retinal ganglion axons for tectal targets explain plasticity of retinotectal projection in the servomechanism model of retinotectal mapping. *Dev. Growth Differ.* **46**, 425-437.
- Janes, P. W., Saha, N., Barton, W. A., Kolev, M. V., Wimmer-Kleikamp, S. H., Nievergall, E., Blobel, C. P., Himanen, J. P., Lackmann, M. and Nikolov, D. B.** (2005). Adam meets Eph. An ADAM substrate recognition module acts as a molecular switch for ephrin cleavage in *trans*. *Cell* **123**, 291-304.
- King, C., Lacey, R., Rodger, J., Barlett, C., Dunlop, S. and Beazley, L.** (2004). Characterization of tectal ephrin-A2 expression during optic nerve regeneration in goldfish: implications for restoration of topography. *Exp. Neurol.* **187**, 380-387.
- Lohof, A. M., Quillan, M., Dan, Y. and Poo, M.** (1992). Asymmetric modulation of cytosolic cAMP activity induces growth cone turning. *J. Neurosci.* **12**, 1253-1261.
- Löschinger, J., Weth, F. and Bonhoeffer, F.** (2000). Reading of concentration gradients by axonal growth cones. *Philos. Trans. R. Soc. Lond. B Biol. Sci.* **355**, 971-982.
- McLaughlin, T. and O'Leary, D. D. M.** (2005). Molecular gradients and development of retinotopic maps. *Annu. Rev. Neurosci.* **28**, 327-355.
- Ming, G., Wong, S. T., Henley, J., Yuan, X., Song, H. J., Spitzer, N. C. and Poo, M.** (2002). Adaptation in the chemotactic guidance of nerve growth cones. *Nature* **417**, 411-418.
- Monschau, B., Kremoser, C., Ohta, K., Tanaka, H., Kaneki, T., Yamada, T., Handwerker, C., Hornberger, M. R., Löschinger, J., Pasquale, E. B. et al.** (1997). Shared and distinct functions of RAGS and ELF-1 in guiding retinal axons. *EMBO J.* **16**, 1258-1267.
- Piper, M., Salih, S., Weinl, C., Holt, C. E. and Harris, W. A.** (2005). Endocytosis-dependent desensitization and protein synthesis-dependent resensitization in retinal growth cone adaptation. *Nat. Neurosci.* **8**, 179-186.
- Prestige, M. C. and Willshaw, D. J.** (1975). On a role for competition in the formation of patterned neural connexions. *Proc. R. Soc. Lond. B Biol. Sci.* **190**, 77-98.
- Quist, A. P., Pavlovic, E. and Oscarsson, S.** (2005). Recent advances in microcontact printing. *Anal. Bioanal. Chem.* **381**, 591-600.
- Rosentreter, S. M., Davenport, R. W., Löschinger, J., Huf, J., Jung, J. and Bonhoeffer, F.** (1998). Response of retinal ganglion cell axons to striped linear gradients of repellent guidance molecules. *J. Neurobiol.* **37**, 541-562.
- Rosoff, W. J., Urbach, J. S., Esrick, M. A., McAllister, R. G., Richards, L. J. and Goodhill, G. J.** (2004). A new chemotaxis assay shows the extreme sensitivity of axons to molecular gradients. *Nat. Neurosci.* **7**, 678-682.
- Song, H. J., Ming, G. and Poo, M.** (1997). cAMP-induced switching in turning direction of nerve growth cones. *Nature* **388**, 275-279.
- Walter, J., Kern-Veits, B., Huf, J., Stolze, B. and Bonhoeffer, F.** (1987). Recognition of position-specific properties of tectal cell membranes by retinal axons in vitro. *Development* **101**, 685-696.
- Weinl, C., Drescher, U., Lang, S., Bonhoeffer, F. and Löschinger, J.** (2003). On the turning of *Xenopus* retinal axons induced by ephrin-A5. *Development* **130**, 1643.
- Xu, J., Rosoff, W. J., Urbach, J. S. and Goodhill, G. J.** (2005). Adaptation is not required to explain the long-term response of axons to molecular gradients. *Development* **132**, 4545-4552.